The Plant Cell, Vol. 26: 3062–3076, July 2014, www.plantcell.org

Insights into the Localization and Function of the Membrane Trafficking Regulator GNOM ARF-GEF at the Golgi Apparatus in *Arabidopsis*[W]

Satoshi Naramoto,[a,b,c,1,2,3] Marisa S. Otegui,[d] Natsumaro Kutsuna,[e] Riet de Rycke,[a] Tomoko Dainobu,[f] Michael Karampelias,[a] Masaru Fujimoto,[g] Elena Feraru,[a,4] Daisuke Miki,[a] Hiroo Fukuda,[f] Akihiko Nakano,[b,f,h] and Jiří Friml[a,i,3]

[a] Department of Plant Systems Biology, VIB, and Department of Plant Biotechnology and Bioinformatics, Ghent University, 9052 Gent, Belgium

[b] Molecular Membrane Biology laboratory, RIKEN Advanced Science Institute, Wako, Saitama 351-0198, Japan

[c] Department of Life Science, International Christian University, Mitaka-shi, Tokyo 181-8585, Japan

[d] Department of Botany and Genetics, University of Wisconsin, Madison, Wisconsin 53706

[e] Department of Integrated Biosciences, Graduate School of Frontier Sciences, University of Tokyo, Kashiwa, Chiba 277-8562, Japan

[f] Department of Biological Sciences, Graduate School of Science, University of Tokyo, Bunkyo-ku, Tokyo 113-0033, Japan

[g] Laboratory of Plant Molecular Genetics, Graduate School of Agricultural and Life Sciences, The University of Tokyo, Bunkyo-ku, Tokyo 113-8657, Japan

[h] Live Cell Molecular Imaging Research Team, Extreme Photonics Research Group, RIKEN Center for Advanced Photonics, Wako, Saitama 351-0198, Japan

[i] Institute of Science and Technology Austria, 3400 Klosterneuburg, Austria

GNOM is one of the most characterized membrane trafficking regulators in plants, with crucial roles in development. GNOM encodes an ARF-guanine nucleotide exchange factor (ARF-GEF) that activates small GTPases of the ARF (ADP ribosylation factor) class to mediate vesicle budding at endomembranes. The crucial role of GNOM in recycling of PIN auxin transporters and other proteins to the plasma membrane was identified in studies using the ARF-GEF inhibitor brefeldin A (BFA). GNOM, the most prominent regulator of recycling in plants, has been proposed to act and localize at so far elusive recycling endosomes. Here, we report the GNOM localization in context of its cellular function in *Arabidopsis thaliana*. State-of-the-art imaging, pharmacological interference, and ultrastructure analysis show that GNOM predominantly localizes to Golgi apparatus. Super-resolution confocal live imaging microscopy identified GNOM and its closest homolog GNOM-like 1 at distinct subdomains on Golgi cisternae. Short-term BFA treatment stabilizes GNOM at the Golgi apparatus, whereas prolonged exposures results in GNOM translocation to *trans*-Golgi network (TGN)/early endosomes (EEs). Malformed TGN/EE in *gnom* mutants suggests a role for GNOM in maintaining TGN/EE function. Our results redefine the subcellular action of GNOM and reevaluate the identity and function of recycling endosomes in plants.

INTRODUCTION

Intracellular membrane trafficking is essential for diverse cellular functions in eukaryotic cells. Both conserved and distinct regulatory systems of vesicle transport have been observed in animal and plant cells. For instances, whereas the *trans*-Golgi network (TGN) is involved in secretion in both animals and plants, the plant TGN also plays roles of early endosomes (EEs) (Dettmer et al., 2006; Robinson et al., 2008). Despite substantial recent advances, the intracellular trafficking system in plant cell is still ill defined compared with animals. The major gap in our understanding of vesicle trafficking in plants is the elusive nature of recycling endosomes, which mediate recycling of proteins from endosomes to the plasma membrane (PM).

ARF-guanine nucleotide exchange factor (GEF) GNOM is the most studied regulator of recycling and a proposed marker for recycling endosomes. ARF-GEFs recruit coat proteins and cargos at the membrane and promote vesicle formation through activation of ARF GTPase by exchanging bound GDP for GTP. In plants, ARF-GEFs are classified in GBF and BIG types, and some of them are sensitive to the fungal toxin brefeldin A (BFA) (Anders and Jürgens, 2008; Naramoto et al., 2010). Among them, BFA-sensitive GNOM ARF-GEF belongs to GBF-type ARF-GEF and plays crucial roles in plant development, in particular, in processes that depend on auxin transport. A weak

[1] Current address: Department of Biological Sciences, Graduate School of Science, University of Tokyo, 7-3-1 Hongo, Bunkyo-ku, Tokyo 113-0033, Japan.

[2] Address correspondence to naramoto@bs.s.u-tokyo.ac.jp.

[3] These authors contributed equally to this work.

[4] Current address: Department of Applied Genetics and Cell Biology, University of Natural Resources and Life Sciences (BOKU), Muthgasse 18, 1190 Vienna, Austria.

The authors responsible for distribution of materials integral to the findings presented in this article in accordance with the policy described in the Instructions for Authors (www.plantcell.org) are: Satoshi Naramoto (naramoto@bs.s.u-tokyo.ac.jp) and Jiří Friml (jiri.friml@ist.ac.at).

[W] Online version contains Web-only data.

www.plantcell.org/cgi/doi/10.1105/tpc.114.125880

allele of *gnom*, also called *vascular network defective7* (*van7*), in *Arabidopsis thaliana* displays fused cotyledons, aberrant patterns of leaf vasculature, no lateral root formation, and root gravitropism defects (Koizumi et al., 2000, 2005; Geldner et al., 2004; Kleine-Vehn et al., 2010). A knockout mutant of *gnom*, also called *embryo defective30* (*emb30*), shows a complete lack of roots and in extreme cases a ball-shaped embryo without defined polarity (Shevell et al., 1994; Steinmann et al., 1999; Geldner et al., 2003). All these phenotypes are related to the auxin transport defective *pin-formed* (*pin*) mutants, suggesting a strong link between GNOM and auxin transport (Gälweiler et al., 1998; Luschnig et al., 1998; Mattsson et al., 1999; Benková et al., 2003; Friml et al., 2003).

Major components of auxin transporter are PIN auxin efflux carriers (Petrásek et al., 2006), mediating the directionality of auxin transport by their polar localization at PMs. They are also the most studied PM cargo proteins for different vesicle trafficking processes. PIN proteins undergo constitutive clathrin-mediated endocytosis and subsequent recycling to different polar domains (Geldner et al., 2001; Dhonukshe et al., 2007; Tanaka et al., 2009; Feraru et al., 2012) or are redirected to the vacuole for degradation (Kleine-Vehn et al., 2008a; Spitzer et al., 2009; Baster et al., 2013). BFA, which is used as an inhibitor of ARF-GEF, blocks the recycling of PIN proteins to the PM, preferentially to the basal side (Kleine-Vehn et al., 2008b), and causes the accumulation of PIN1 proteins in the aggregating GNOM-positive intracellular compartments (Geldner et al., 2003). Notably, seedlings expressing engineered version of GNOM whose BFA sensitivity is engineered from sensitive to insensitive do not show PIN trafficking defects after BFA treatment (Geldner et al., 2003). In addition, mislocalization of basally localized PIN proteins is also observed in *gnom* mutants (Steinmann et al., 1999; Kleine-Vehn et al., 2008b). These results established the crucial role of GNOM in recycling and provide the rationale for the auxin-related patterning phenotypes of *gnom* mutants (Geldner et al., 2003). They also firmly established a role for GNOM within the presumptive recycling endosomes of plants.

Besides its endosomal recycling function, a minor portion of GNOM was revealed to regulate endocytosis at the PM (Naramoto et al., 2010). In addition, GNOM can compensate for ARF-GEF defects at the Golgi apparatus. Mutation in the BFA-resistant *GNOM-Like1* (*GNL1*) gene, the closest homolog of GNOM, causes secretion defects (Richter et al., 2007; Teh and Moore, 2007). Just like GBF-type ARF-GEFs in yeasts and mammals, GNL1 is localized to the Golgi apparatus (Peyroche et al., 2001; D'Souza-Schorey and Chavrier, 2006; Bui et al., 2009). Surprisingly, the expression of an extra copy of *GNOM* under the control of the *GNL1* promoter rescued the *gnl1* mutants (Richter et al., 2007). Furthermore, whereas *gnl1* seedlings have morphologically abnormal Golgi stacks in the presence of BFA, introduction of engineered BFA-resistant GNOM can rescue this defect in *gnl1* (Richter et al., 2007). These results indicate that, besides its recycling endosomal function, GNOM can act at the Golgi apparatus if GNL1 function is compromised or GNOM is overexpressed.

These results have been critical to our understanding of GNOM functions in different vesicle trafficking processes. However, there are still many open questions on the roles of GNOM in subcellular trafficking. One of the main unresolved issues is the exact subcellular localization of GNOM and, thus, the identity of the elusive recycling endosomes. GNOM has not been convincingly shown to colocalize with any known subcellular markers under undisturbed conditions. Previous studies suggested that GNOM does not localize to the Golgi apparatus, TGN/EE, or prevacuolar compartment/multivesicular body (MVB), whereas GNOM-GFP (green fluorescent protein) clearly colocalized with both TGN/EE and prevacuolar compartment/MVB marker proteins when seedlings were treated with BFA (Geldner et al., 2003; Grebe et al., 2003; Dettmer et al., 2006; Jaillais et al., 2006). The absence of colocalization of GNOM with known subcellular markers as well as the lack of reliable marker proteins that define recycling endosomes has raised the question as to the identity of plant recycling endosomes open. To define plant recycling endosomes and to provide further insights into GNOM function, we performed a detailed analysis of the subcellular localization of GNOM in *Arabidopsis*. Contrasting with the current paradigm of GNOM localization at recycling endosomes, we found that GNOM preferentially localizes to a subdomain of the Golgi apparatus and redefined a role of this organelle in regulating endosomal function.

RESULTS

GNOM-GFP-Labeled Organelles Are Not Efficiently Stained with the Endocytosis Tracer FM4-64

GNOM-GFP-labeled organelles are reported to be stained with the endocytosis tracer FM4-64 (Jelínková et al., 2010), suggesting that GNOM localizes to endosomal compartments (Geldner et al., 2003). However, temporal information on when FM4-64 starts to stain GNOM-GFP-labeled compartments as well as the extent of the colocalization is lacking. Moreover, the timing of FM4-64 colocalization with early endosomal markers suggested that GNOM localized to a later compartment on the endosomal pathway (Dettmer et al., 2006). To further characterize the GNOM-GFP-labeled organelles in the context of endocytosis pathway, we performed a detailed FM4-64 uptake analysis in the roots of *pGNOM:GNOM-GFP* seedlings (Geldner et al., 2003). First, we applied 2 μM FM4-64 to GNOM-GFP seedlings for 5 min at 4°C, intensively washed out the dye, and followed its localization. As previously shown, GNOM-GFP showed weak localization at the PM (Naramoto et al., 2010) and prominent intracellular signals (Geldner et al., 2003) (Figure 1; Supplemental Figure 1). The intracellular GNOM-GFP organelles were not efficiently stained with FM4-64 after 6 or 30 min incubation. This is sufficient time for the FM4-64 dye to reach the TGN/EE because control experiments showed that the TGN/EE marker Vacuolar H^+-ATPase a1 (VHA-a1)-GFP was strongly stained after 6 min (Figures 1A, 1B, and 1D; Supplemental Figures 1A to 1F). Surprisingly, we did not observe colocalization even after 90 min incubation, when FM4-64 had already trafficked to the vacuolar membrane (Figures 1C and 1D; Supplemental Figures 1G to 1I). Altogether, these results indicate that, following uptake of FM4-64 at the PM and subsequent endocytic trafficking, FM4-64 did not pass through GNOM-positive compartments,

suggesting that GNOM does not localize primarily to early or late endosomal compartments.

GNOM-Positive Compartments Show Similar Morphology to the Golgi Apparatus

The finding that GNOM-GFP-labeled compartments were not efficiently stained with FM4-64 raised a question about their identity. To better characterize the organelles where GNOM is localized, we analyzed our samples by variable-angle epifluorescence microscopy (VAEM), which can provide more structural details than conventional confocal laser scanning microscopy (CLSM) (Fujimoto et al., 2007; Konopka et al., 2008). Previous observations detected functional GNOM-GFP at dot-like structures at the cell surface (Naramoto et al., 2010). To better observe the GNOM-GFP-labeled intracellular structures, we changed the angle of excitation laser to preferentially observe the intracellular signals. We found GNOM-GFP-labeled ring-like structures that move by cytoplasmic streaming (Figure 2A). We compared the VAEM images of GNOM localization with those of several organelle markers, including the Golgi marker ST-mRFP (monomeric red fluorescent protein), the TGN/EE marker VHA-a1-mRFP, and the MVB marker mRFP-ARA7 (Naramoto et al., 2009, 2014). Similar to the GNOM-GFP-labeled structures, ST-mRFP labeled the ring-like structures that moved along the cells, whereas VHA-a1-mRFP and mRFP-ARA7 labeled dot-like structures (Figures 2B to 2D). These results revealed similarities between GNOM-GFP-labeled compartments and the Golgi stacks.

GNOM-GFP Localizes to the ST-mRFP-Labeled Organelles

VAEM analyses implied a close relationship between GNOM-GFP-labeled organelles and the Golgi stacks. To elucidate where GNOM is localized within the cell, RFP-tagged organelle marker lines were crossed with the *emb30/gnom* mutant rescued with the transgene *pGNOM:GNOM-GFP* and were observed by CLSM. Excitation of GNOM-GFP using high laser intensity detected occasional weak signals at the PM as reported previously (Naramoto et al., 2010). However, this approach hampers the detailed observation of intracellular structures. Therefore, to analyze the intracellular structures, we used lower laser intensity, not allowing for the detection of the PM GNOM-GFP signal. This approach identified that dot-like signals of GNOM-GFP were not significantly colocalized with the TGN/EE marker, VHA-a1-mRFP (Crowell et al., 2009) (Figures 3A and 3D; Supplemental Figures 2A to 2C), or with the MVB marker, mRFP-ARA7 (Ueda et al., 2004) (Figures 3B and 3D; Supplemental Figures 2D to 2F). By contrast, significant colocalization was observed between GNOM-GFP and the Golgi marker, ST-mRFP (Teh and Moore, 2007) (Figures 3C and 3D; Supplemental Figures 2G to 2I). RT-PCR analysis of *GNOM-GFP* expression detected similar expression levels of *GNOM-GFP* compared with endogenous *GNOM* (Supplemental Figure 3), suggesting that we observe correct subcellular localization of GNOM. These results suggest that GNOM is localized to Golgi apparatus.

To further confirm GNOM localization at the Golgi apparatus, we performed CLSM imaging of pharmacologically treated seedlings expressing GNOM-GFP and RFP-tagged organelle marker lines. First, we tested the effect of Concanamycin A (ConcA), an inhibitor of V-ATPase that is known to cause enlargement of the TGN (Dettmer et al., 2006; Robinson et al., 2008). After treatment with 2 μM ConcA for 1 h, the morphology of the GNOM-GFP-labeled compartment was not dramatically changed, whereas VHA-a1-labeled TGN/EE was enlarged (Figures 3E; Supplemental Figures 4A to 4C). These data also suggest that GNOM is not localized to the TGN/EE.

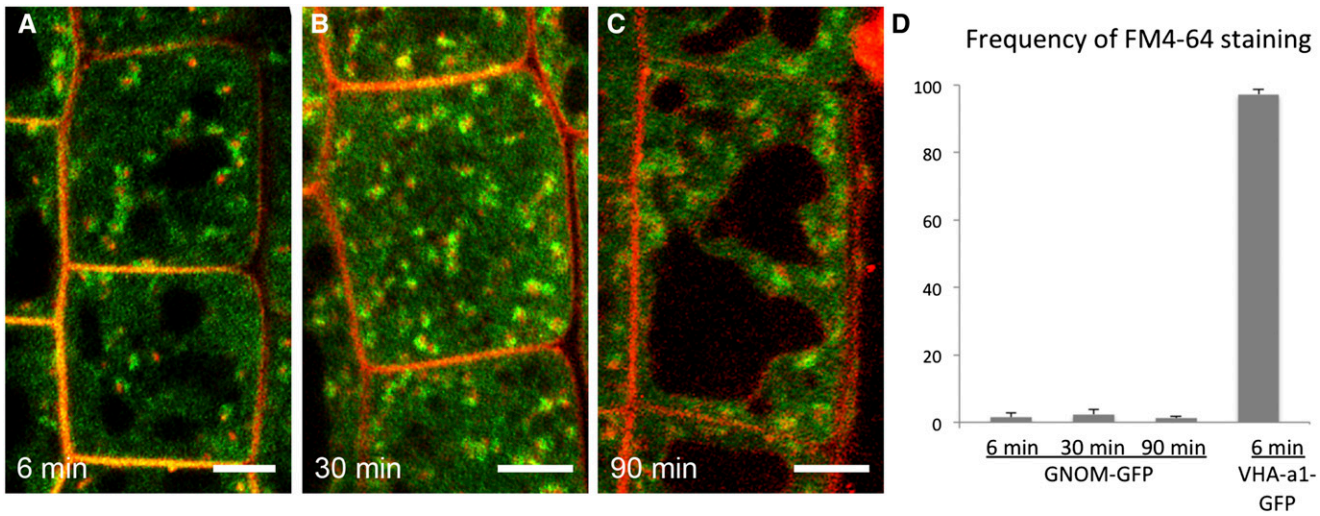

Figure 1. GNOM-GFP-Labeled Compartments Are Not Efficiently Stained by FM4-64.

(A) to **(C)** Representative confocal images of root epidermal cells labeled with FM4-64 (red) and GNOM-GFP (green). The time after the start of incubation with FM4-64 is indicated on each panel. Bars = 3 μm.

(D) Quantification of the colocalization ratio between GNOM-GFP and FM4-64. Most of the GNOM-GFP-labeled structures are not stained by FM4-64, even at a time when FM4-64 reaches the vacuoles, whereas the TGN/EE marker, VHA-a1-GFP, is strongly colocalized with FM4-64. Error bars indicate the SD values for data from three independent experiments. At least 200 GNOM-GFP-labeled organelles were analyzed in each experiment.

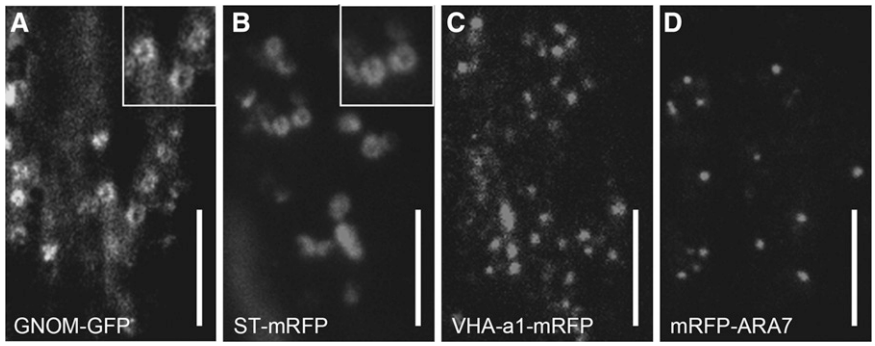

Figure 2. GNOM-GFP Localizes to Ring-Like Structures Reminiscent of the Golgi Apparatus.

VAEM micrographs of root epidermal cells expressing GNOM-GFP **(A)**, ST-mRFP **(B)**, VHA-a1-mRFP **(C)**, and mRFP-ARA7 **(D)**. Insets of **(A)** and **(B)** represent enlarged view of organelles that show ring-like structures. Bars = 3 μm.

Next, we tested wortmannin (Wm), an inhibitor of phosphatidyl inositol-3-OH kinase activity. Wm causes swelling of MVB without significantly affecting the morphology of the Golgi apparatus and TGN/EE (Jaillais et al., 2006, 2008; Robinson et al., 2008). The morphology of the organelles labeled by GNOM-GFP did not change after 1 h treatment with 50 μM Wm, whereas ARA7-labeled MVBs were swollen (Figure 3F; Supplemental Figures 4D to 4F). These results suggest that GNOM does not localize to MVBs.

Finally, we tested the effect of monensin, a monovalent cation ionophore that exchanges Na^+, K^+, and H^+ across membranes.

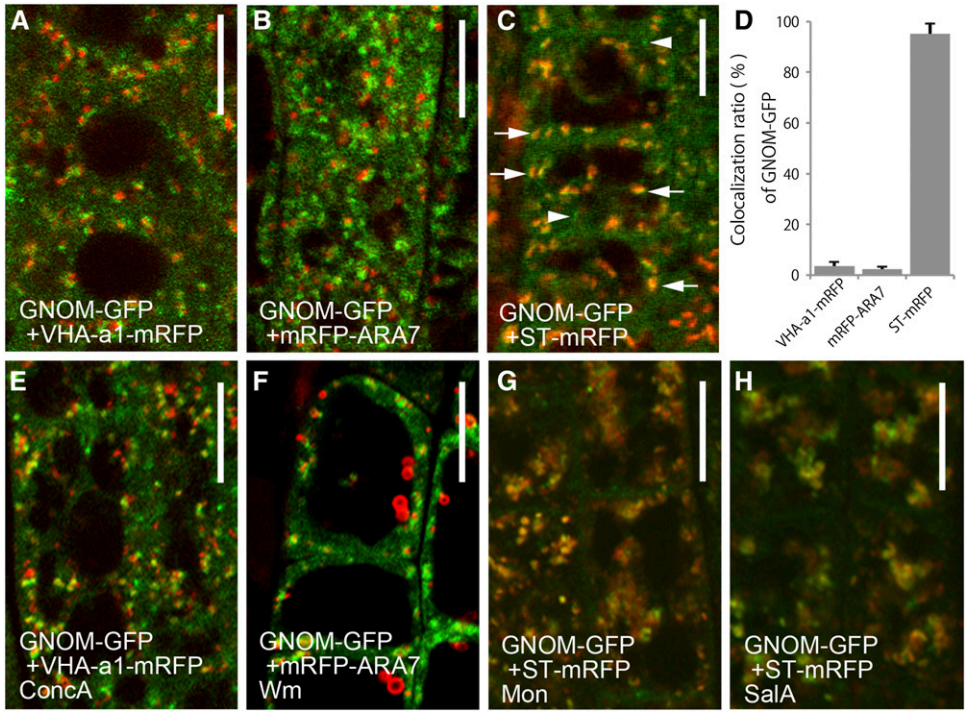

Figure 3. GNOM-GFP Localizes Primarily to the Golgi Apparatus.

(A) to **(D)** Double labeling of GNOM-GFP (green) and subcellular markers tagged with RFP (red) in normal conditions. Compared with VHA-a1-mRFP **(A)** and mRFP-ARA7 **(B)**, GNOM-GFP localizes to distinct compartments. GNOM-GFP colocalizes with the Golgi marker, ST-mRFP **(C)**. The colocalization percentage is shown in **(D)**. Arrows and arrowheads indicate ST-mRFP-positive and -negative GNOM-GFP-labeled compartments, respectively. Error bars indicate the SD values for data from three independent experiments. At least 200 GNOM-GFP-labeled organelles were analyzed in each experiment.
(E) to **(H)** Response of GNOM-GFP and RFP-tagged organelle markers to pharmacological interference. Root cells expressing GNOM-GFP treated with ConcA **(E)**, Wm **(F)**, monensin (Mon) **(G)**, and salinomycin A (SalA) **(H)**. For testing the effectiveness of chemicals, VHA-a1-mRFP **(E)**, mRFP-ARA7 **(F)**, and ST-mRFP (**[G]** and **[H]**) were used as a control. Treatment with Mon and SalA was performed for 30 min; treatment with ConcA and Wm was performed for 1 h. The distribution of GNOM-GFP changes after Mon and SalA treatments.
Bars = 8 μm.

Monensin has been widely used to study the functions of the Golgi apparatus in animals (Tartakoff, 1983; Farquhar, 1985), and there are reports that monensin causes swelling of the Golgi apparatus and TGN in plant cells (Zhang et al., 1993). After treatment with 10 μM monensin for 30 min, GNOM-GFP-labeled compartments and ST-mRFP-labeled Golgi apparatus were strongly enlarged and were also colocalized (Figure 3G; Supplemental Figures 4G to 4I). Similar results (Figure 3H; Supplemental Figures 4J to 4L) were obtained when we applied 10 μM salinomycin for 30 min, a monovalent cation ionophore that is assumed to function similarly to monensin (Chen-Pan et al., 1999). We also confirmed that the Golgi marker, ST-mRFP, behaves in a similar manner to GNOM-GFP after treatment with the Wm and ConcA (Supplemental Figures 5A to 5C). Altogether, these results further support the notion that GNOM is localized to the Golgi apparatus.

Super-Resolution Imaging Identifies the Differential Localization of GNOM and GNL1 at the Golgi Apparatus

GNL1, the closest homolog of GNOM, localizes to the Golgi apparatus and regulates the transport of coat protein complex I (COPI)-coated vesicles (Richter et al., 2007; Teh and Moore, 2007). Although *gnom* and *gnl1* mutants display distinct cellular and morphological phenotypes, expression of an extra copy of *GNOM* complements the phenotype of *gnl1* mutants, suggesting a functional relationship between GNOM and GNL1 (Richter et al., 2007). Therefore, we performed subcellular localization analysis of GNOM and GNL1. We established transgenic lines expressing functional *pGNL1:GNL1-TagRFP* and compared the subcellular localization with functional *pGNOM:GNOM-GFP*. CLSM observation of functional GNOM-GFP and functional GNL1-TagRFP revealed colocalization, which further confirmed the Golgi localization of GNOM (Figures 4A to 4C). Closer observation revealed slightly different localization of GNOM-GFP and GNL1-TagRFP at the Golgi apparatus; however, due to the limitations in the spatial resolution of CLSM, the exact suborganellar localization of GNOM and GNL1 at the Golgi stacks could not be resolved (Figures 4D to 4F).

We have developed a high-performance 3D confocal microscopy system, called super-resolution confocal live imaging microscopy (SCLIM), which combines spinning-disk confocal scanning, electron multiplying charge-coupled device cameras, and deconvolution (Matsuura-Tokita et al., 2006; Ito et al., 2012; Kurokawa et al., 2013). A comparison of conventional CLSM and SCLIM using yeast (*Saccharomyces cerevisiae*) Golgi showed that CLSM identified flat disk-like structures, whereas SCLIM could resolve the fenestrated morphology of Golgi apparatus as seen by electron microscopy (Matsuura-Tokita et al., 2006). Therefore, we used SCLIM to investigate how GNOM and GNL1 cooperate at the Golgi apparatus.

First, we tested the applicability of SCLIM to observe plant Golgi stacks. Plant Golgi stacks consist of closely appressed disk-like cisternae, which are defined as *cis*, medial, and *trans* cisternae (Neumann et al., 2003; Staehelin and Kang, 2008; Faso et al., 2009). Dual-color 3D SCLIM imaging of the *cis*-Golgi marker ERD2-GFP and the *trans*-Golgi marker ST-mRFP (Boevink et al., 1998) allows for the spatial separation of the *cis* and *trans* sides of individual Golgi stacks (Supplemental Figure 6A), indicating that this is suitable imaging approach for analyzing protein localization within Golgi stacks. When GNOM-GFP and GNL1-TagRFP were observed using this system, although both of them localized at the same Golgi stacks, their signals were partially overlapping but clearly segregated within a single Golgi stack (Figures 4G to 4I). This suborganellar localization could not be resolved by conventional CLSM (Figures 4D to 4F). This distinct separation of GFP and RFP signals was not an artifact of deconvolution because ST-GFP- and ST-mRFP-labeled *trans*-Golgi cisternae displayed almost completely identical patterns (Supplemental Figure 6B). Furthermore, we could observe the ring-like localization of GNOM-GFP on the Golgi cisternae, which suggests that GNOM localizes at the margin of the flat disk-like Golgi cisternae (Figures 4G to 4I; Supplemental Figure 6C). GNL1 also was observed at the margin, but it had a less prominent ring-like localization. Taken together, these results

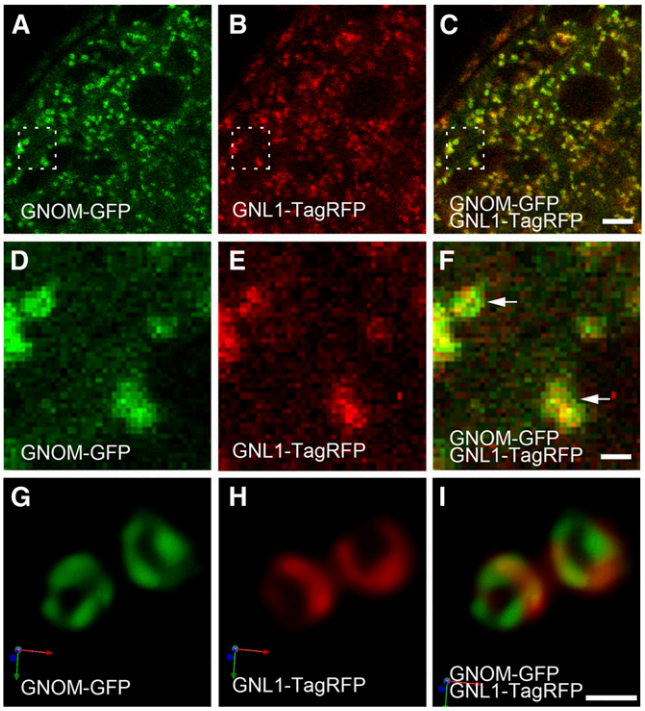

Figure 4. GNOM and GNL1 Localize to Distinct Regions within the Golgi Apparatus.

(A) to **(F)** CLSM micrographs of *Arabidopsis* root cells coexpressing GNOM-GFP (green) and GNL1-TagRFP (red). GNOM-GFP **(A)** and GNL1-TagRFP **(B)** colocalize to the Golgi apparatus. A merged image is shown in **(C)**. Enlarged views of the dashed frames in **(A)** to **(C)** are shown in **(D)** to **(F)**, respectively. Arrows indicate the apparent distinct localization of GNOM-GFP and GNL1-TagRFP.

(G) to **(I)** SCLIM micrographs of *Arabidopsis* root cells that coexpress GNOM-GFP and GNL1-TagRFP. High-resolution confocal analysis identified distinct but partially overlapping subcellular localization of GNOM-GFP **(G)** and GNL1-TagRFP **(H)** at the periphery of the Golgi cisternae. A merged image is shown in **(I)**. Images are shown in 3D display and arrows indicate the *xyz* axis.

Bars = 4 μm for **(A)** to **(C)** and 600 nm for **(D)** to **(I)**.

indicated the distinct suborganellar localization of GNOM and GNL1 on the Golgi apparatus and imply that ARF-GEF GNOM is preferentially active at the margin of Golgi cisternae.

Transmission Electron Microscopy of Immunogold-Labeled Cryosections Confirm the Golgi Localization of GNOM-GFP

To further verify GNOM localization at the Golgi apparatus, we performed immunogold electron microscopy (IEM) analysis using anti-GFP antibodies on high-pressure frozen/freeze-substituted roots expressing GNOM-GFP. We detected a weak signal at the Golgi in untreated root cells (Figures 5A, 5B, and 5E; Supplemental Figure 7), and this signal was enhanced by treatment with 50 μM BFA for 3 min (Figures 5C to 5E; Supplemental Figure 8). By contrast, we could not detect equally strong GFP labeling at the TGN or MVB in either untreated seedlings or seedlings treated with BFA for 3 min. As expected, no significant immunogold labeling of GFP antibody at the Golgi apparatus was detected in wild-type seedlings (Figure 5E; Supplemental Figure 9). These results further confirmed localization of GNOM ARF-GEF at the Golgi apparatus.

BFA Treatment Induces Translocation of GNOM from the Golgi to the TGN

GNOM localizes on intracellular endomembranes and, to a lesser extent, the PM (Geldner et al., 2003; Naramoto et al., 2010). In addition to these locations, as typical for ARF-GEFs,

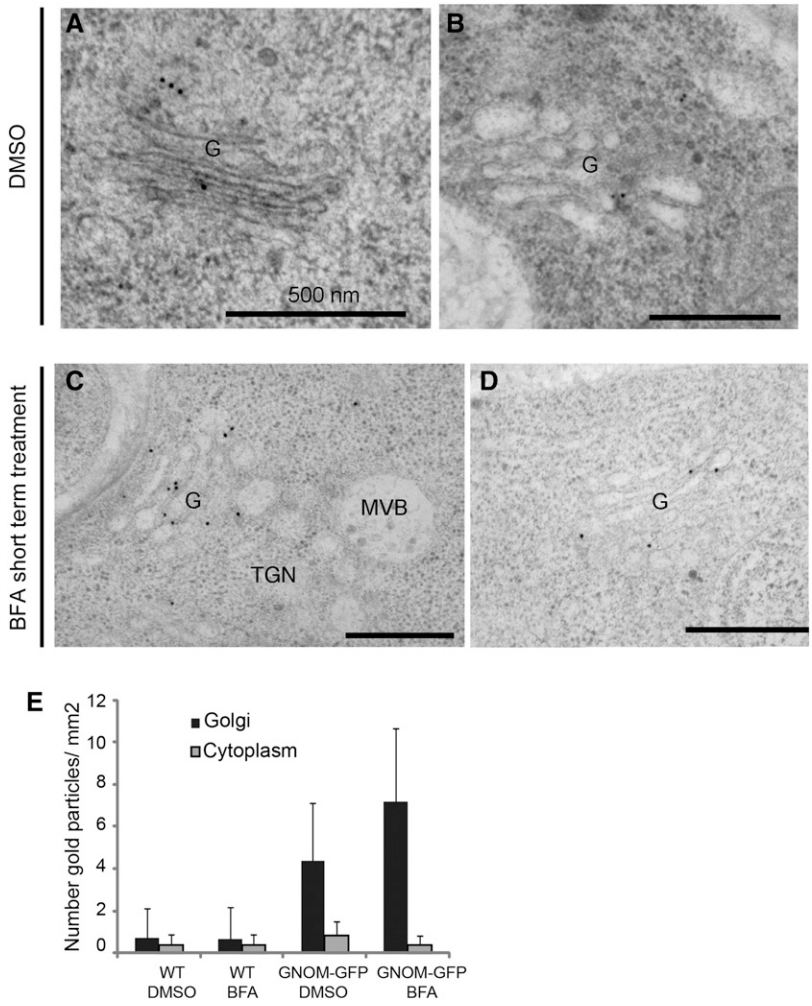

Figure 5. IEM Analysis Identifies GNOM-GFP at the Golgi Apparatus.

(A) to **(D)** IEM analysis of GNOM-GFP with anti-GFP antibodies. GNOM-GFP is localized to the Golgi apparatus in DMSO- (**[A]** and **[B]**) and BFA-treated (**[C]** and **[D]**) cells at the ultrastructural levels.

(E) Quantification analysis of GNOM-GFP localization. Quantification confirmed that GNOM localization at the Golgi apparatus is enhanced after short-term BFA treatment. Error bars indicate SD. Between 20 and 30 Golgi stacks from at least 10 cells in two independent roots were considered for this analysis. Note the weaker or absent detection of GNOM-GFP at the TGN and MVB under either BFA-treated or untreated conditions. The Golgi apparatus is designated as "G" within the figure.

Bars = 500 nm.

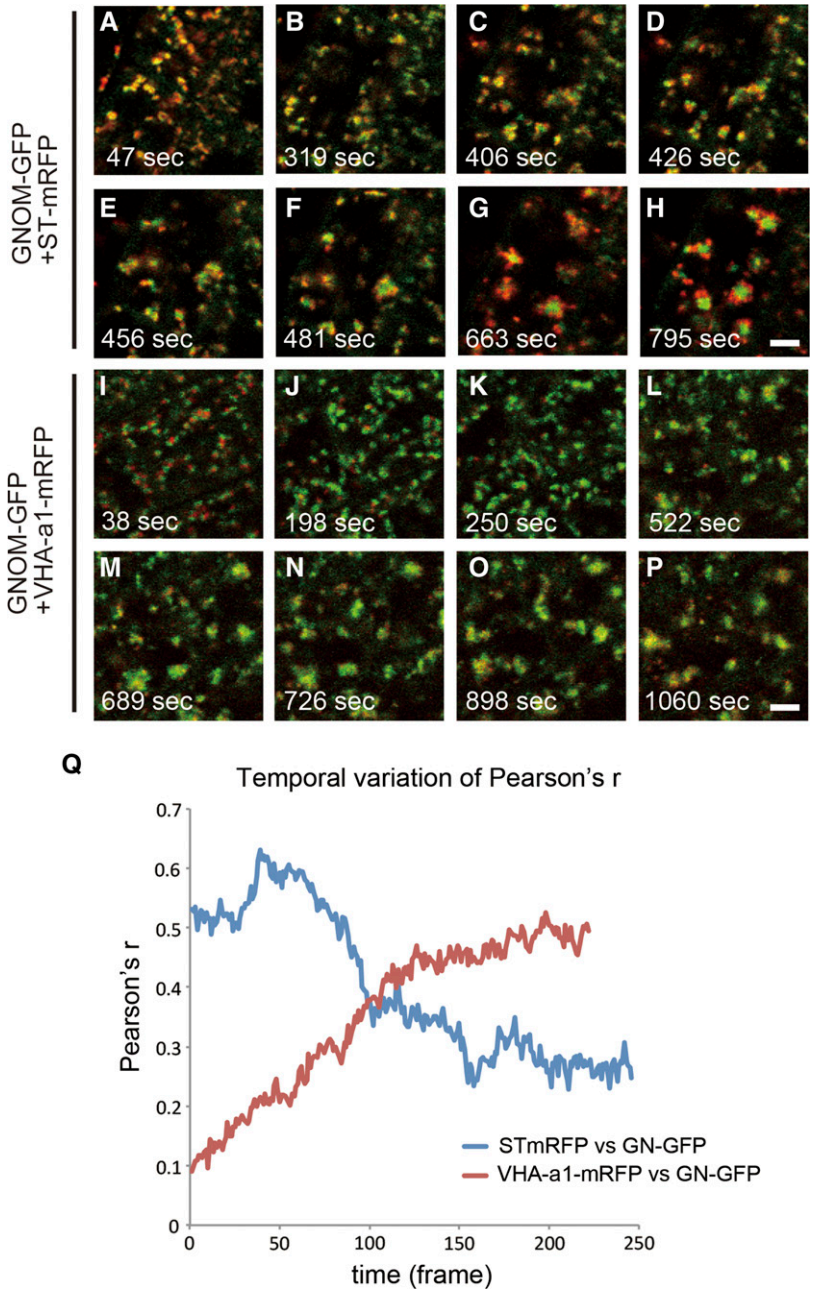

Figure 6. GNOM-GFP Translocates from the Golgi Apparatus to the TGN after BFA Treatment.

(A) to **(H)** Double labeling of GNOM-GFP (green) with ST-mRFP (red) in BFA-treated root tip cells. BFA incubation times are indicated at the lower corner.

(I) to **(P)** Double labeling of GNOM-GFP (green) with VHA-a1-mRFP (red) in BFA-treated root tip cells. BFA incubation times are indicated at the lower corner.

(Q) Time-course quantification of the colocalization ratio between GNOM-GFP and ST-mRFP or VHA-a1-mRFP. Note the clear segregation of GNOM-GFP- and VHA-a1-mRFP-labeled structures at the earliest time points, whereas GNOM-GFP and VHA-a1-mRFP gradually colocalize during subsequent incubation. The initial complementary colocalization of GNOM with ST-mRFP gradually segregates.

Bars = 4 μm.

GNOM is also localized to the cytosol, which often hampers subcellular localization analysis (Geldner et al., 2003). BFA is known to stabilize the BFA-sensitive ARF-GEFs at the membranes where they act (Zeghouf et al., 2005), providing a means to analyze subcellular localization and place of action of BFA-sensitive ARF-GEFs (Geldner et al., 2003; Naramoto et al., 2010). Using this approach, it has been repeatedly reported that BFA-sensitive GNOM localizes at endosomes that aggregate at the core of the BFA body in the presence of BFA (Geldner et al., 2003; Grebe et al., 2003; Jaillais et al., 2006). However, in the absence or 3 min application of BFA, our results suggest that GNOM is localized to the Golgi apparatus. To elucidate this apparent inconsistency, we performed dual-color live-cell imaging analysis between GNOM-GFP and ST-mRFP or VHA-a1-mRFP in the presence of 50 μM BFA. After 1 min BFA incubation (the earliest technically possible time point), most of the GNOM-GFP was localized to the ST-mRFP-labeled Golgi stacks, which agrees with our current data (Figure 6A). However, at the later time points, surprisingly, GNOM-GFP gradually translocated from the STmRFP-labeled Golgi stacks to the core of the BFA body, in agreement with the previous observations (Geldner et al., 2003) (Figures 6A to 6H and 6Q; Supplemental Movie 1). In contrast, GNOM-GFP and VHA-a1-mRFP showed different localization patterns at the early time points (Figure 6I) but gradually colocalized at later time points, and by 18 min in BFA, they were colocalized at the core of the BFA body (Figures 6I to 6P; Supplemental Movie 2). We also analyzed the subcellular localization of MYC-tagged GNOM by immunofluorescence. We failed to detect signals in BFA-untreated cells, suggesting the technical difficulty in immunostaining of GNOM-MYC, possibly caused by the instability of GNOM-MYC during fixation; however, treatment with BFA for 5 min stabilized GNOM-MYC at the Golgi apparatus, which then translocated to the TGN after 1 h BFA treatment (Supplemental Figure 10). These results indicate that BFA treatment initially stabilizes GNOM at the Golgi apparatus and then causes the gradual translocation of GNOM from the Golgi to the TGN/EE. These observations fully reconcile the apparently contradicting observations regarding GNOM localization at endosomes versus the Golgi.

BFA Treatment Does Not Efficiently Translocate Engineered BFA-Resistant GNOM from the Golgi Apparatus

GNL1 localizes to the Golgi apparatus under both control and BFA treatment conditions (Richter et al., 2007). We showed that, unlike GNL1, BFA-sensitive GNOM translocated from the Golgi to the TGN in the presence of BFA. In *Arabidopsis*, *GNL1* encodes a BFA-resistant ARF-GEF, whereas *GNOM* encodes a BFA-sensitive ARF-GEF (Geldner et al., 2003; Richter et al., 2007). We hypothesized that this distinct BFA sensitivity of GNOM and GNL1 may be the cause of the differences in their response to BFA treatment. The sensitivity or resistance to BFA can be changed by introducing a point mutation, without affecting the overall function of ARF-GEF (Peyroche et al., 1999). To test our hypothesis, we established *gnl1gn* double mutants expressing constructs for both engineered BFA-sensitive GNL1-YFP and BFA-resistant GNOM-MYC (Geldner et al., 2003; Richter et al., 2007) and analyzed their subcellular localization. Consistent with previous reports, engineered BFA-sensitive GNL1-YFP colocalized with the Golgi-localized γCOPI protein detected by immunofluorescence (Richter et al., 2007) (Supplemental Figures 11A to 11C). However, similar to wild-type (BFA-sensitive) GNOM (Figure 6), after 50 μM BFA treatment for 1 h, it translocated from the Golgi apparatus to the center of the BFA body, where it colocalized with PIN1 (Supplemental Figures 11D to 11F and 12). By contrast, engineered BFA-resistant GNOM-MYC under the same conditions remained at the periphery of the BFA body, where it localized at the Golgi stacks, labeled by the anti-γCOPI antibody (Figures 7A to 7D; Supplemental Figures 11G to 11I). These results indicate that BFA treatment translocates BFA-sensitive but not BFA-resistant ARF-GEFs from the Golgi to endosomes and further strengthen our notion that, similar to GNL1, GNOM is preferentially localized to the Golgi apparatus under normal conditions.

GNOM Function Affects the Properties of the TGN/EE

Previous cell biological analysis identified a crucial role of GNOM in recycling of basally localized PIN proteins and other PM cargos, including polysaccharides (Steinmann et al., 1999; Shevell et al., 2000). This is somewhat difficult to reconcile with its Golgi localization. To elucidate the subcellular function of GNOM, we performed a combination of CLSM and transmission electron microscopy (TEM) analysis in the roots of weak *gnomR5* and *van7* alleles (Koizumi et al., 2000; Geldner et al., 2004). First, we analyzed the distribution of ARF1-GFP, which localizes primarily at the TGN and to a lesser extent at the Golgi apparatus (Paciorek et al., 2005; Xu and Scheres, 2005; Tanaka et al., 2009; Robinson et al., 2011). In wild-type plants, the ARF1-GFP signal showed punctate distribution throughout the cells (Figure 8A). By contrast, ARF1-GFP-labeled organelles were either aggregated or enlarged in some *gnomR5* cells (Figure 8B), which is reminiscent of BFA-induced changes in intracellular compartments (Lee et al., 2010; Grebe et al., 2003). Notably, these affected organelles were stained by FM4-64, indicating that TGN/EE compartments aggregate or become enlarged in *gnom* mutant cells (Figure 8B). Detailed morphological

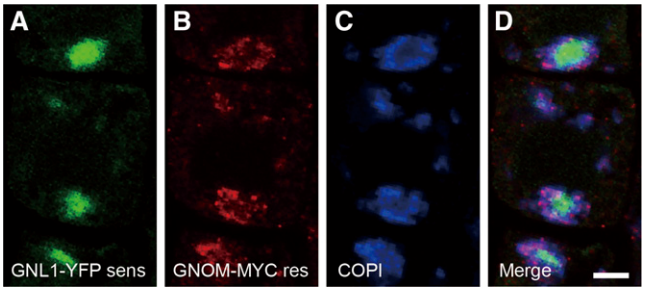

Figure 7. Engineered BFA-Sensitive GNL1 Translocates from the Golgi Apparatus to the TGN.

Triple labeling of BFA-sensitive GNL1-YFP (green) **(A)**, BFA-resistant GNOM-MYC (red) **(B)**, and anti-COPI antibody (blue) **(C)** in BFA-treated root epidermal cells expressing functional *BFA-sensitive GNL1-YFP* and *BFA-resistant GNOM-MYC* lines. A merged image is shown in **(D)**. Note the endosomal localization of BFA-sensitive GNL1-YFP, but the Golgi localization of BFA-resistant GNOM-MYC. Bar = 4 μm.

analysis by TEM identified that TGN/EE at the *trans*-Golgi surface of *van7* and *gnomR5*, weak alleles of *gnom*, often showed highly vesiculated TGN/EE profiles (Figures 8C and 8D, Table 1; Supplemental Figure 13). Furthermore, these Golgi/TGN complexes are often clustered in *van7* and *gnomR5* mutants (Table 1). These results suggest that GNOM function is necessary for maintaining the proper TGN/EE distribution or structure, despite being predominantly localized at the Golgi apparatus, which would be also consistent with the originally proposed role of GNOM in protein recycling.

DISCUSSION

GNOM ARF-GEF Preferentially Localizes to the Golgi Apparatus

GNOM is a well-characterized trafficking regulator that is crucial for development. The recycling defects of PM cargos following interference with GNOM function suggest GNOM action at recycling endosomes (Geldner et al., 2003). Recently, BFA-visualized exocytic trafficking defective5 (BEX5), a RabA1 trafficking regulator, has also been shown to mediate recycling of the PM cargos in *Arabidopsis* (Feraru et al., 2012). However, *bex5* mutants, in contrast to *gnom* mutants, did not display pronounced developmental defects, so its biological role is still unclear. Altogether, GNOM is believed to be a main factor regulating recycling of PM cargos.

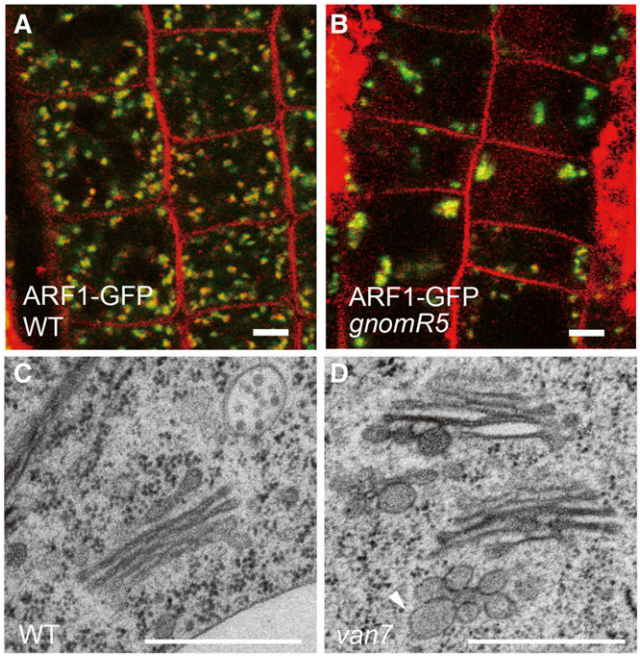

Figure 8. Abnormal Morphology or Distribution of TGN/EE Is Observed in *gnom* Mutants.

(A) and **(B)** CLSM image of ARF1-GFP (green) and FM4-64 (red) signals in wild-type **(A)** and *gnomR5* **(B)** root cells. ARF1-GFP-labeled structures are enlarged or aggregated in *gnomR5* mutants **(B)**.
(C) and **(D)** TEM image of wild-type **(C)** and *van7* **(D)** root cells. TGN/EE with highly vesiculated profiles in *van7* mutants **(D)**. Arrowhead indicates vesiculated TGN/EE.
Bars = 4 μm for **(A)** and **(B)** and 500 nm for **(C)** and **(D)**.

Table 1. Characterization of TGN/EE and GA Distribution Patterns for Various Mutants

	Number of Analyzed GAs	Number of Highly Vesiculated TGN/EE Profiles	Number of Clustered Golgi
Wild type	36	3 (8.3%)	2 (5.6%)
van7	33	21 (63.6%)	13 (39.4%)
gnomR5	18	13 (72.2%)	10 (55.5%)

TGN/EE located within 150 to 200 nm from GAs (Golgi apparatus) were analyzed. Highly vesiculated TGN/EE profiles corresponded to TGN/EE with pronounced budding/fusing vesicles in single TEM sections. Numbers between parentheses represents percentage of GAs associated with highly vesiculated TGN/EE. "Clustered GA" is defined as the Golgi stacks located within 450 to 600 nm from each other. Numbers between parentheses represent percentage of clustered GAs.

Previous analysis indicated that the endocytic tracer FM4-64 stained GNOM-GFP-positive organelles. Furthermore, following inhibition by BFA, functional GNOM-MYC colocalized with endosomal markers (Geldner et al., 2003). Based on these results, GNOM was widely believed to localize and function at yet to be identified recycling endosomes. However, most GNOM localization studies were done only after BFA treatment and not in undisturbed situations. Also, the FM4-64 staining results are not conclusive. Other studies failed to detect colocalization between FM4-64 and GNOM under normal conditions (Chow et al., 2008). These issues indicate that the available experimental data are not sufficient to define the subcellular localization of GNOM.

Here, our analyses using multiple imaging approaches demonstrate that GNOM localizes predominantly at the Golgi apparatus. Super-resolution microscopy revealed that GNOM-positive organelles show morphology and behavior similar to those of the Golgi apparatus. Detailed CLSM analysis identified that GNOM-GFP-positive organelles are labeled by Golgi markers but not by FM4-64, even after FM4-64 was distributed throughout the whole endocytic pathway (Figures 1 and 3). Ultrastructural analysis confirmed GNOM-GFP localization at the Golgi apparatus (Figure 5). Importantly, time-lapse imaging identified that BFA caused the translocation of GNOM ARF-GEF from the Golgi apparatus to the TGN/EE, showing that prolonged BFA treatment causes GNOM mislocalization (Figure 6; Supplemental Figure 10 and Supplemental Movies 1 and 2). This explains the apparent inconsistencies with previous observations (Geldner et al., 2003). All these data strongly suggest that GNOM localizes preferentially at the Golgi apparatus.

GNOM Mislocalization after BFA Treatment

The main source of confusion in establishing the place of GNOM action has been the mislocalization of GNOM after prolonged BFA treatment. Our time-lapse imaging and immunolocalization analysis demonstrate that, although GNOM is stabilized at the Golgi apparatus shortly after the BFA treatment, GNOM gradually translocates from the Golgi apparatus to the TGN/EE after

prolonged BFA treatments (Figures 5 and 6; Supplemental Figure 10). This phenomenon is due to the BFA action on GNOM because an engineered BFA-resistant GNOM remained at the Golgi apparatus even after prolonged BFA treatment (Figure 7). Importantly, we also report the translocation of engineered BFA-sensitive GNL1, closest homolog of GNOM, from the Golgi apparatus to the TGN/EE under BFA treatment (Figure 7; Supplemental Figures 11 and 12). These results show that BFA treatment causes the translocation of BFA-sensitive ARF-GEFs from the Golgi apparatus to the TGN/EE.

What is the underlying mechanism of such translocation? TGN tends to localize in the close proximity of *trans*-Golgi cisternae (Dettmer et al., 2006) and moves together within the cell (Viotti et al., 2010), which suggested they may interact closely. Electron tomography analysis suggested the TGN arise from the *trans*-Golgi cisternae by means of a cisternal peeling (Staehelin and Kang, 2008). However, detailed live-cell imaging analysis identified both Golgi-associated TGN and Golgi-independent TGN, which suggested TGN is an independent organelle from the Golgi apparatus (Uemura et al., 2014). Furthermore, TGN functions as EE. Thus, this complex nature of TGN/EE makes it challenging to understand the mechanism of GNOM translocation. Future experiments will be needed to analyze the nature of the plant TGN/EE. However, in any case, a large portion of the TGN/EE is closely associated with the *trans* surface of the Golgi apparatus, and membrane flow from the Golgi apparatus to the TGN/EE occurs during secretion. It is conceivable that GNOM protein, which is stabilized at the Golgi membranes by BFA, can automatically be transported to the TGN/EE as long as the Golgi remains operational.

Super-Resolution Microscopy Provides Insights into the Differential Localization and Function of *Arabidopsis* Gea/GBF-Type ARF-GEFs

GNOM and GNL1 are the closest homologs in *Arabidopsis*, and they belong to the GBF-type ARF-GEFs that regulate vesicle formation at the Golgi apparatus in yeast and mammals (Gillingham and Munro, 2007). Notwithstanding their structural similarity, they possess both redundant and distinct functions. The *gnom* mutants show defective endocytic recycling of PIN1 proteins, whereas *gnl1* mutants display defects in secretion but not in general endocytic recycling (Steinmann et al., 1999; Teh and Moore, 2007). Conversely, genetic experiments showed that expression of *pGNL1:GNOM* can rescue *gnl1* mutants, suggesting functional redundancy. These findings seem somewhat inconsistent and raise questions about the functional relationship between GNOM and GNL1.

Our super-resolution CLSM analysis revealed that GNOM and GNL1 localized to spatially different regions within the same Golgi stacks, consistent with the occurrence of at least multiple secretory systems within the Golgi (Figure 4). Consistently, previous studies showed that the secretion of secGFP (secreted green fluorescent protein) and cell wall matrix polysaccharides, both of which are transported through the Golgi apparatus, depend on different secretory machineries in tobacco (*Nicotiana tabacum*) (Leucci et al., 2007). In addition, *gnom* and *gnl1* mutants show defective transport of polysaccharides and secGFP, respectively, and GNOM is not largely involved in the transport of secGFP (Shevell et al., 2000; Teh and Moore, 2007). It is tempting to speculate that GNOM and GNL1 preferentially regulate the transport of different cargos at their own Golgi domains. In contrast, functional redundancy between the two proteins may be explained if we assume that overproduced GNOM protein leaks into the GNL1 domains and consequently is able to take over its function.

Our super-resolution CLSM system also provided additional insights into the localization of ARF-GEF proteins at the periphery of the Golgi cisternae. Fluorescently tagged GNOM and GNL1 localized to ring-like structures (Figures 4G to 4I). COPI vesicles are formed at the rims of Golgi cisternae by ARF-GEF action and COPI shows a similar ring-like distribution at the Golgi (Pimpl et al., 2000). These results, and our own observations, suggest that GNOM and GNL1 also localize and

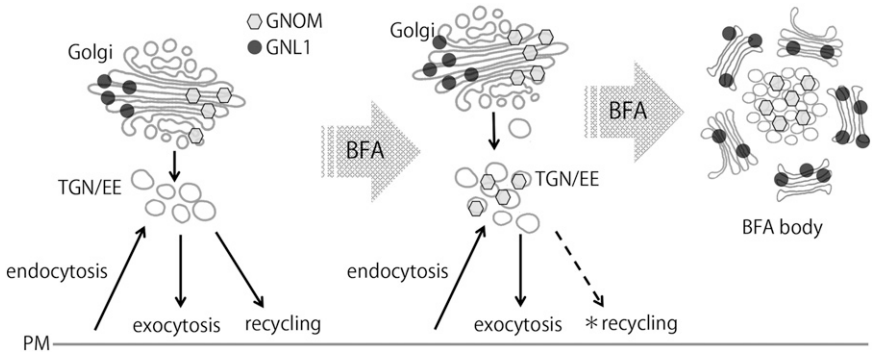

Figure 9. Model of Intracellular Trafficking System in Plants and the Response to BFA.

BFA-sensitive GNOM localizes with BFA-resistant GNL1 to distinct but partially overlapping subdomains of the Golgi apparatus. GNOM regulates vesicle budding at the Golgi apparatus and indirectly regulate recycling of PM cargos through maintaining the function of TGN/EE. TGN or its subdomain is a good candidate for recycling endosomes. BFA causes gradual translocation of GNOM from Golgi stacks to TGN/EE. During this process, BFA indirectly inhibit recycling pathways (marked by asterisk). Minor population of GNOM and GNL1 also revealed to localize at PMs to mediate endocytosis. Dotted arrows represent the inhibited trafficking pathway.

function at the periphery of Golgi cisternae. This observation is in agreement with our own electron microscopy analysis and with previous reports (Richter et al., 2007) (Figure 5; Supplemental Figures 7 and 8). These results suggest that GNOM and GNL1 ARF-GEFs differentially localize to the rims of Golgi cisternae where they presumably regulate COPI-dependent vesicle formation.

What Is the Cellular Function of GNOM?

Current models about GNOM places its main function at recycling endosomes (Geldner et al., 2003), whereas a minor portion of GNOM at the PM regulates endocytosis (Naramoto et al., 2010). In this article, we identified that GNOM primarily localizes at Golgi apparatus instead of distinct recycling endosomes. Based on these results, we propose that GNOM at the Golgi apparatus indirectly regulates the recycling of PIN and other proteins to the PM (Figure 9). We cannot completely rule out that GNOM localizes to other organelles not detected in our analysis, including recycling endosomes, but it could only be a very small fraction of the total GNOM pool. Our cell biological analysis identified that the TGN/EE tends to be highly vesiculated in *gnom* mutants, which suggests a role for GNOM in the maintenance of TGN/EE structure and possibly also its function (Figure 8). Because TGN/EE is supposed to closely interact with the Golgi apparatus (Staehelin and Kang, 2008), it is not surprising that defects in Golgi-localized proteins, such as GNOM, can compromise TGN/EE function. Considering the fact that TGN regulates both endocytic and secretory trafficking (Viotti et al., 2010), the TGN (or a TGN subdomain) is a good candidate for recycling endosomes in plants (Figure 9). Recent subcellular localization analysis identified partial colocalization of the GTPase RabA and VHA-a1 on the TGN membrane, suggesting the existence of functionally distinct TGN subdomains, which may be specialized for secretion and endocytosis (Chow et al., 2008; Naramoto et al., 2014). It is tempting to speculate that PIN protein is endocytosed to the TGN and then recycles back to the PM through the TGN-based secretory pathway.

The localization of GNOM at the Golgi apparatus and its function in recycling might seem difficult to reconcile. However, every organelle is interconnected by continuous membrane transport; thus, the outcome of ARF-GEF inhibition is often observed at the place where the corresponding ARF-GEF does not localize. For example, in animals, endosomal structure and function, such as transcytosis, is affected by BFA (Hunziker et al., 1991; Lippincott-Schwartz et al., 1991; Wood et al., 1991), although all endosomal ARF-GEFs are BFA resistant (Frank et al., 1998; Franco et al., 1999; Someya et al., 2001). This clearly indicates that ARF-GEF function is not necessarily directly correlated with its subcellular localization. Furthermore, identification of BEN1/MIN7, the TGN/EE-localized ARF-GEF, whose mutants do not efficiently internalize PIN proteins following BFA treatment, suggests more complex ARF-GEF-dependent endocytic routes (Tanaka et al., 2009). To address the scenario that GNOM indirectly regulates TGN/EE function and thereby the recycling of PM cargos, it will be necessary to better characterize endocytic and recycling trafficking pathways and to identify the involved endomembrane compartments, including recycling endosomes, if such specialized and distinct structures exist in plants.

In summary, we found that the majority of GNOM ARF-GEFs localized with GNL1 to distinct but partially overlapping subdomains of the Golgi. We also showed that GNOM relocate from Golgi to TGN/EE after BFA treatment. Finally, our data suggested a role for GNOM in the maintenance of TGN/EE structure, thereby providing a possible explanation for the role of GNOM in recycling. Our findings present more refined model for action of this developmentally essential trafficking regulator (Figure 9) and provide unexpected insights into the regulation of TGN/EE-based processes by the Golgi apparatus.

METHODS

Plant Material and Growth Conditions

Arabidopsis thaliana seedlings harboring the following transgenes had been described previously: *pGNOM:GNOM-GFP*, *BFA-resistant GNOM-MYC*, *BFA-sensitive GNL1-MYC* and *BFA-sensitive GNL1-YFP* as well as the *Arabidopsis* mutants *van7* and *gnom*^{R5} (Koizumi et al., 2000; Geldner et al., 2003, 2004; Richter et al., 2007). All the *pGNOM:GNOM-GFP*, *pGNOM:GNOM-MYC*, and *pGNL1:GNL1-XFP* constructs were expressed in their own mutants and tested for functionality. To perform double labeling experiments between GNOM and any organelle marker lines, *emb30* knockout mutant seedlings that express both functional *pGNOM:GFP* (or functional *pGNOM:MYC*) and organelle markers genes were used to prevent the overexpression of GNOM. Plant transformation was performed using the floral dip method (Clough and Bent, 1998). To perform experiments, seeds were sown on 0.8% agar-solidified 0.5× Murashige and Skoog medium supplemented with 1% sucrose (pH 5.9) at 18°C and a 16-h-light/8-h-dark cycle, unless otherwise indicated.

Generation of *pGNL1:GNL1TagRFP* Construct

TagRFP sequence was amplified by PCR from the Gateway TagRFP-AS-N plasmid (Evrogen). The *GNL1-TagRFP* construct was made using the triple-template PCR method (Tian et al., 2004) with 3× [(Gly_3)Ser]-TagRFP sequence and 10-kb genomic fragment of GNL1 that contains 2 kb upstream and 1.5 kb downstream, as template. The *GNL1-TagRFP* construct was cloned into pENTR D-TOPO (Invitrogen) and then transferred to pH7WG Gateway destination vector (Karimi et al., 2002) by LR Clonase II (Invitrogen).

Quantitative RT-PCR

Total RNA was isolated from 5-d-old seedlings using an RNeasy mini kit (Qiagen). The quantitative RT-PCR was performed using a Light Cycler 1.2 apparatus (Roche). The primers and probes used for RT-PCR were designed by the website for the Universal ProbeLibrary Assay Design Center (https://qpcr.probefinder.com/input.jsp?organism=a_tha). Quantitative RT-PCR was conducted using the first-strand cDNA, synthesized by SuperScript III RT (Invitrogen) with oligo(dt)20 primers, as a template with the LightCycler Taqman Master System (Roche). The relative mRNA levels were normalized by the concentration of At-*MBF1A* as a reference gene. The data used were the average of three replicates.

Antibody Staining and Confocal Laser Scanning Microscopy

Whole-mount immunolocalization on *Arabidopsis* roots was done with an automated system (Intavis in situ pro) as described previously (Paciorek et al., 2006). Antibodies were diluted as follows: rabbit anti-PIN1 (1:2000) and Cy3-conjugated secondary anti-rabbit (1:600; Sigma-Aldrich) antibodies. For FM4-64 labeling of *Arabidopsis* seedling roots, 4- to 5-d-old

seedlings were pulse labeled in liquid medium containing 2 μM FM4-64 for 5 min at 4°C and washed in liquid media. Immunofluorescence and live-cell microscopy were done with an Olympus FV1000.

Inhibitor Treatment

Root cells expressing GNOM-GFP were incubated in solid Murashige and Skoog medium containing the respective inhibitor or corresponding amount of solvent. The following stock solutions were used: 50 mM BFA in DMSO, 10 mM ConcA in DMSO, 10 mM monensin in DMSO, 10 mM salinomycin in DMSO, and 20 mM Wm in DMSO. Treatment with Mon and SalA was performed for 30 min and treatment with ConcA and Wm was performed for 1 h.

High-Resolution 3D Imaging

A custom-made system produced by the Dynamic-Bio Project was used. In this system, an Olympus IX-70 microscope was equipped with a special high signal-to-noise-ratio color confocal system (Yokogawa Electric), image intensifiers (Hamamatsu Photonics), and electron multiplying charge-coupled device cameras (NHK Engineering Service and Hitachi Kokusai Electric). In both settings, an Ar^+/Kr^+ laser (Melles Griot) was used to excite GFP at 488 nm and RFP at 568 nm simultaneously. For 3D imaging, the objective lens was oscillated vertically to the sample plane by a piezo actuator system (Yokogawa Electric). Collected pictures were analyzed with Volocity software (Improvision). Deconvolution analysis was also performed with Volocity using theoretical point-spread functions.

Transmission Electron Microscopy

Root tips of 4-d-old seedlings of *Arabidopsis* were excised, immersed in 20% (w/v) BSA, and frozen immediately in a high-pressure freezer (EM PACT; Leica Microsystems). Freeze substitution was performed using a Leica EM AFS (Leica Microsystems) in dry acetone containing 0.1% uranylcetate, 1% (w/v) OsO_4, and 0.2% glutaraldehyde over a 4-d period as follows: −90°C for 54 h, 2°C per hour increase for 15 h, −60°C for 8 h, 2°C per hour increase for 15 h, and −30°C for 8 h. Samples were then slowly warmed up to 4°C, infiltrated stepwise over 3 d at 4°C in Spurr's resin and embedded in capsules. The polymerization was performed at 70°C for 16 h. Ultrathin sections were made using an ultramicrotome (Leica EM UC6) and poststained in a Leica EM AC20 for 40 min in uranyl acetate at 20°C and for 10 min in lead stain at 20°C. Grids were viewed with a JEM 1010 transmission electron microscope (JEOL) operating at 80 kV.

For immunolabeling of GNOM-GFP in *Arabidopsis*, roots of 8-d-old wild-type and GNOM-GFP seedlings were incubated for 3 min in either 50 μM BFA in 0.1% DMSO and 0.1 M sucrose or just in 0.1% DMSO and 0.1 M sucrose and high-pressure frozen in a Baltec HPM 010 high-pressure freezer. Frozen samples were substituted in 0.2% uranyl acetate (Electron Microscopy Sciences) plus 0.2% glutaraldehyde (Electron Microscopy Sciences) in acetone at −80°C for 72 h and warmed to −50°C for 24 h. After several acetone rinses, these samples were infiltrated with Lowicryl HM20 (Electron Microscopy Sciences) for 72 h and polymerized at −50°C under UV light for 48 h. Sections were mounted on Formvar-coated nickel grids and blocked for 20 min with a 5% (w/v) solution of nonfat milk in Tris-buffered saline containing 0.1% Tween 20. The sections were incubated in the primary polyclonal antibodies anti-GFP for 3 h, rinsed in Tris-buffered saline containing 0.5% Tween 20, and then transferred to the secondary antibody (anti-rabbit IgG 1:10) conjugated to 15-nm gold particles for 1 h. Two roots of each genotype and treatment were used for immunogold labeling. Gold particle distribution was analyzed using Fiji/ImageJ (http://pacific.mpi-cbg.de/wiki/index.php/Fiji).

Accession Numbers

Sequence data from this article can be found in the GenBank/EMBL library under the following accession numbers: ARA7 (At4g19640), ARF1 (At1g23490), BEX5/RabA1b (At1g16920), COPI (T75984), GNOM (At1g13980), GNL1 (At5g39500), MIN7 (At3g43300), PIN1 (At1g73590), ST (AJ243198), and VHA-a1 (At2g28520).

Supplemental Data

The following materials are available in the online version of this article.

Supplemental Figure 1. GNOM-GFP Is Less Efficiently Stained by the Endocytosis Tracer FM4-64.

Supplemental Figure 2. The Distribution of GNOM-GFP and RFP-Tagged Organelle Markers.

Supplemental Figure 3. Quantitative RT-PCR Analysis of *GNOM-GFP* Expression.

Supplemental Figure 4. The Distribution of GNOM-GFP and RFP-Tagged Organelle Markers in Response to Pharmacological Interference.

Supplemental Figure 5. The Distribution of ST-mRFP Is Not Strongly Affected by Concanamycin and Wortmannin.

Supplemental Figure 6. High-Resolution Microscopy Observation Systems Succeeded in Observing the Plant Golgi Apparatus.

Supplemental Figure 7. GNOM-GFP Localizes to the Golgi Apparatus in BFA-Untreated Root Cells.

Supplemental Figure 8. GNOM-GFP Localizes to the Golgi Apparatus in BFA-Treated Root Cells.

Supplemental Figure 9. An Anti-GFP Antibody Does Not Stain the Golgi Apparatus.

Supplemental Figure 10. GNOM-MYC Is Stabilized at the Golgi Apparatus during Short-Term BFA Treatment and Subsequently Localizes at the TGN during Mid-Term BFA Treatment.

Supplemental Figure 11. Engineered BFA-Sensitive Functional GNL1-YFP Translocates from the Golgi Apparatus to Endosomes following BFA Treatment.

Supplemental Figure 12. PIN1 Is Internalized by the Inhibition of GNL1 Function.

Supplemental Figure 13. TGN Structure Is Malformed in *van7* and *gnomR5* Mutants.

Supplemental Movie 1. Live-Cell Imaging of *Arabidopsis* Root Cells Expressing GNOM-GFP and ST-mRFP in the Presence of BFA.

Supplemental Movie 2. Live-Cell Imaging of *Arabidopsis* Root Cells Expressing GNOM-GFP and VHA-a1-mRFP in the Presence of BFA.

ACKNOWLEDGMENTS

We thank Gerd Jürgens, Ian Moore, Ben Scheres, Karin Schumacher, and David Robinson for providing published materials and the ABRC and NASC for seed stocks. We also thank Jürgen Kleine-vehn, Stephanie Robert, Hirokazu Tanaka, and Takashi Ueda for helpful discussions and Martine De Cock for help in preparing the article. This work was supported by the Japanese Society for the Promotion of Science (30612022 to S.N. and 24770038 to N.K.), the NC-CARP project of the Ministry of Education, Culture, Sports, Science, and Technology in Japan to S.N. and H.F., the Odysseus Program of the Research Foundation-Flanders (J.F.), EMBO (LTF 795-2012) to E.F., and National Science Foundation Grant MCB1157824 to M.S.O.

AUTHOR CONTRIBUTIONS

S.N. carried out main parts of the confocal microscopy experiments. M.S.O. conducted IEM. R.d.R. carried out TEM. N.K. carried out the quantification analysis presented in Figure 6. M.F. conducted VAEM. S.N., T.D., M.K., E.F., D.M., H.F., and A.N. analyzed data. S.N., M.S.O., T.D., and J.F. wrote the article. S.N. and J.F. supervised the study; thus, S.N. and J.F. contributed equally to this work.

Received March 31, 2014; revised May 28, 2014; accepted June 4, 2014; published July 10, 2014.

REFERENCES

Anders, N., and Jürgens, G. (2008). Large ARF guanine nucleotide exchange factors in membrane trafficking. Cell. Mol. Life Sci. **65:** 3433–3445.

Baster, P., Robert, S., Kleine-Vehn, J., Vanneste, S., Kania, U., Grunewald, W., De Rybel, B., Beeckman, T., and Friml, J. (2013). SCF(TIR1/AFB)-auxin signalling regulates PIN vacuolar trafficking and auxin fluxes during root gravitropism. EMBO J. **32:** 260–274.

Benková, E., Michniewicz, M., Sauer, M., Teichmann, T., Seifertová, D., Jürgens, G., and Friml, J. (2003). Local, efflux-dependent auxin gradients as a common module for plant organ formation. Cell **115:** 591–602.

Boevink, P., Oparka, K., Santa Cruz, S., Martin, B., Betteridge, A., and Hawes, C. (1998). Stacks on tracks: the plant Golgi apparatus traffics on an actin/ER network. Plant J. **15:** 441–447.

Bui, Q.T., Golinelli-Cohen, M.P., and Jackson, C.L. (2009). Large Arf1 guanine nucleotide exchange factors: evolution, domain structure, and roles in membrane trafficking and human disease. Mol. Genet. Genomics **282:** 329–350.

Chen-Pan, C., Pan, I.J., Yamamoto, Y., Sakogawa, T., Yamada, J., and Hayashi, Y. (1999). Prompt recovery of damaged adrenal medullae induced by salinomycin. Toxicol. Pathol. **27:** 563–572.

Chow, C.M., Neto, H., Foucart, C., and Moore, I. (2008). Rab-A2 and Rab-A3 GTPases define a trans-golgi endosomal membrane domain in Arabidopsis that contributes substantially to the cell plate. Plant Cell **20:** 101–123.

Clough, S.J., and Bent, A.F. (1998). Floral dip: a simplified method for Agrobacterium-mediated transformation of *Arabidopsis thaliana*. Plant J. **16:** 735–743.

Crowell, E.F., Bischoff, V., Desprez, T., Rolland, A., Stierhof, Y.D., Schumacher, K., Gonneau, M., Höfte, H., and Vernhettes, S. (2009). Pausing of Golgi bodies on microtubules regulates secretion of cellulose synthase complexes in Arabidopsis. Plant Cell **21:** 1141–1154.

Dettmer, J., Hong-Hermesdorf, A., Stierhof, Y.D., and Schumacher, K. (2006). Vacuolar H^+-ATPase activity is required for endocytic and secretory trafficking in Arabidopsis. Plant Cell **18:** 715–730.

Dhonukshe, P., Aniento, F., Hwang, I., Robinson, D.G., Mravec, J., Stierhof, Y.D., and Friml, J. (2007). Clathrin-mediated constitutive endocytosis of PIN auxin efflux carriers in Arabidopsis. Curr. Biol. **17:** 520–527.

D'Souza-Schorey, C., and Chavrier, P. (2006). ARF proteins: roles in membrane traffic and beyond. Nat. Rev. Mol. Cell Biol. **7:** 347–358.

Farquhar, M.G. (1985). Progress in unraveling pathways of Golgi traffic. Annu. Rev. Cell Biol. **1:** 447–488.

Faso, C., Boulaflous, A., and Brandizzi, F. (2009). The plant Golgi apparatus: last 10 years of answered and open questions. FEBS Lett. **583:** 3752–3757.

Feraru, E., Feraru, M.I., Asaoka, R., Paciorek, T., De Rycke, R., Tanaka, H., Nakano, A., and Friml, J. (2012). BEX5/RabA1b regulates trans-Golgi network-to-plasma membrane protein trafficking in Arabidopsis. Plant Cell **24:** 3074–3086.

Franco, M., Peters, P.J., Boretto, J., van Donselaar, E., Neri, A., D'Souza-Schorey, C., and Chavrier, P. (1999). EFA6, a sec7 domain-containing exchange factor for ARF6, coordinates membrane recycling and actin cytoskeleton organization. EMBO J. **18:** 1480–1491.

Frank, S., Upender, S., Hansen, S.H., and Casanova, J.E. (1998). ARNO is a guanine nucleotide exchange factor for ADP-ribosylation factor 6. J. Biol. Chem. **273:** 23–27.

Friml, J., Vieten, A., Sauer, M., Weijers, D., Schwarz, H., Hamann, T., Offringa, R., and Jürgens, G. (2003). Efflux-dependent auxin gradients establish the apical-basal axis of Arabidopsis. Nature **426:** 147–153.

Fujimoto, M., Arimura, S.-i., Nakazono, M., and Tsutsumi, N. (2007). Imaging of plant dynamin-related proteins and clathrin around the plasma membrane by variable incidence angle fluorescence microscopy. Plant Biotechnol. **24:** 449–455.

Gälweiler, L., Guan, C., Müller, A., Wisman, E., Mendgen, K., Yephremov, A., and Palme, K. (1998). Regulation of polar auxin transport by AtPIN1 in Arabidopsis vascular tissue. Science **282:** 2226–2230.

Geldner, N., Anders, N., Wolters, H., Keicher, J., Kornberger, W., Muller, P., Delbarre, A., Ueda, T., Nakano, A., and Jürgens, G. (2003). The Arabidopsis GNOM ARF-GEF mediates endosomal recycling, auxin transport, and auxin-dependent plant growth. Cell **112:** 219–230.

Geldner, N., Friml, J., Stierhof, Y.D., Jürgens, G., and Palme, K. (2001). Auxin transport inhibitors block PIN1 cycling and vesicle trafficking. Nature **413:** 425–428.

Geldner, N., Richter, S., Vieten, A., Marquardt, S., Torres-Ruiz, R.A., Mayer, U., and Jürgens, G. (2004). Partial loss-of-function alleles reveal a role for GNOM in auxin transport-related, post-embryonic development of Arabidopsis. Development **131:** 389–400.

Gillingham, A.K., and Munro, S. (2007). The small G proteins of the Arf family and their regulators. Annu. Rev. Cell Dev. Biol. **23:** 579–611.

Grebe, M., Xu, J., Möbius, W., Ueda, T., Nakano, A., Geuze, H.J., Rook, M.B., and Scheres, B. (2003). Arabidopsis sterol endocytosis involves actin-mediated trafficking via ARA6-positive early endosomes. Curr. Biol. **13:** 1378–1387.

Hunziker, W., Whitney, J.A., and Mellman, I. (1991). Selective inhibition of transcytosis by brefeldin A in MDCK cells. Cell **67:** 617–627.

Ito, Y., Uemura, T., Shoda, K., Fujimoto, M., Ueda, T., and Nakano, A. (2012). cis-Golgi proteins accumulate near the ER exit sites and act as the scaffold for Golgi regeneration after brefeldin A treatment in tobacco BY-2 cells. Mol. Biol. Cell **23:** 3203–3214.

Jaillais, Y., Fobis-Loisy, I., Miège, C., and Gaude, T. (2008). Evidence for a sorting endosome in Arabidopsis root cells. Plant J. **53:** 237–247.

Jaillais, Y., Fobis-Loisy, I., Miège, C., Rollin, C., and Gaude, T. (2006). AtSNX1 defines an endosome for auxin-carrier trafficking in Arabidopsis. Nature **443:** 106–109.

Jelínková, A., Malínská, K., Simon, S., Kleine-Vehn, J., Parezová, M., Pejchar, P., Kubes, M., Martinec, J., Friml, J., Zazímalová, E., and Petrásek, J. (2010). Probing plant membranes with FM dyes: tracking, dragging or blocking? Plant J. **61:** 883–892.

Karimi, M., Inzé, D., and Depicker, A. (2002). GATEWAY vectors for Agrobacterium-mediated plant transformation. Trends Plant Sci. **7:** 193–195.

Kleine-Vehn, J., Ding, Z., Jones, A.R., Tasaka, M., Morita, M.T., and Friml, J. (2010). Gravity-induced PIN transcytosis for polarization of auxin fluxes in gravity-sensing root cells. Proc. Natl. Acad. Sci. USA **107:** 22344–22349.

Kleine-Vehn, J., Leitner, J., Zwiewka, M., Sauer, M., Abas, L., Luschnig, C., and Friml, J. (2008a). Differential degradation of PIN2 auxin efflux carrier by retromer-dependent vacuolar targeting. Proc. Natl. Acad. Sci. USA **105:** 17812–17817.

Kleine-Vehn, J., Dhonukshe, P., Sauer, M., Brewer, P.B., Wiśniewska, J., Paciorek, T., Benková, E., and Friml, J. (2008b). ARF GEF-dependent transcytosis and polar delivery of PIN auxin carriers in Arabidopsis. Curr. Biol. **18:** 526–531.

Koizumi, K., Sugiyama, M., and Fukuda, H. (2000). A series of novel mutants of *Arabidopsis thaliana* that are defective in the formation of continuous vascular network: calling the auxin signal flow canalization hypothesis into question. Development **127:** 3197–3204.

Koizumi, K., Naramoto, S., Sawa, S., Yahara, N., Ueda, T., Nakano, A., Sugiyama, M., and Fukuda, H. (2005). VAN3 ARF-GAP-mediated vesicle transport is involved in leaf vascular network formation. Development **132:** 1699–1711.

Konopka, C.A., Backues, S.K., and Bednarek, S.Y. (2008). Dynamics of Arabidopsis dynamin-related protein 1C and a clathrin light chain at the plasma membrane. Plant Cell **20:** 1363–1380.

Kurokawa, K., Ishii, M., Suda, Y., Ichihara, A., and Nakano, A. (2013). Live cell visualization of Golgi membrane dynamics by super-resolution confocal live imaging microscopy. Methods Cell Biol. **118:** 235–242.

Lee, O.R., Kim, S.J., Kim, H.J., Hong, J.K., Ryu, S.B., Lee, S.H., Ganguly, A., and Cho, H.T. (2010). Phospholipase A(2) is required for PIN-FORMED protein trafficking to the plasma membrane in the Arabidopsis root. Plant Cell **22:** 1812–1825.

Leucci, M.R., Di Sansebastiano, G.P., Gigante, M., Dalessandro, G., and Piro, G. (2007). Secretion marker proteins and cell-wall polysaccharides move through different secretory pathways. Planta **225:** 1001–1017.

Lippincott-Schwartz, J., Yuan, L., Tipper, C., Amherdt, M., Orci, L., and Klausner, R.D. (1991). Brefeldin A's effects on endosomes, lysosomes, and the TGN suggest a general mechanism for regulating organelle structure and membrane traffic. Cell **67:** 601–616.

Luschnig, C., Gaxiola, R.A., Grisafi, P., and Fink, G.R. (1998). EIR1, a root-specific protein involved in auxin transport, is required for gravitropism in *Arabidopsis thaliana*. Genes Dev. **12:** 2175–2187.

Matsuura-Tokita, K., Takeuchi, M., Ichihara, A., Mikuriya, K., and Nakano, A. (2006). Live imaging of yeast Golgi cisternal maturation. Nature **441:** 1007–1010.

Mattsson, J., Sung, Z.R., and Berleth, T. (1999). Responses of plant vascular systems to auxin transport inhibition. Development **126:** 2979–2991.

Naramoto, S., Nodzyński, T., Dainobu, T., Takatsuka, H., Okada, T., Friml, J., and Fukuda, H. (2014). VAN4 encodes a putative TRS120 that is required for normal cell growth and vein development in Arabidopsis. Plant Cell Physiol. **55:** 750–763.

Naramoto, S., Sawa, S., Koizumi, K., Uemura, T., Ueda, T., Friml, J., Nakano, A., and Fukuda, H. (2009). Phosphoinositide-dependent regulation of VAN3 ARF-GAP localization and activity essential for vascular tissue continuity in plants. Development **136:** 1529–1538.

Naramoto, S., Kleine-Vehn, J., Robert, S., Fujimoto, M., Dainobu, T., Paciorek, T., Ueda, T., Nakano, A., Van Montagu, M.C., Fukuda, H., and Friml, J. (2010). ADP-ribosylation factor machinery mediates endocytosis in plant cells. Proc. Natl. Acad. Sci. USA **107:** 21890–21895.

Neumann, U., Brandizzi, F., and Hawes, C. (2003). Protein transport in plant cells: in and out of the Golgi. Ann. Bot. (Lond.) **92:** 167–180.

Paciorek, T., Sauer, M., Balla, J., Wiśniewska, J., and Friml, J. (2006). Immunocytochemical technique for protein localization in sections of plant tissues. Nat. Protoc. **1:** 104–107.

Paciorek, T., Zazímalová, E., Ruthardt, N., Petrásek, J., Stierhof, Y.D., Kleine-Vehn, J., Morris, D.A., Emans, N., Jürgens, G., Geldner, N., and Friml, J. (2005). Auxin inhibits endocytosis and promotes its own efflux from cells. Nature **435:** 1251–1256.

Petrásek, J., et al. (2006). PIN proteins perform a rate-limiting function in cellular auxin efflux. Science **312:** 914–918.

Peyroche, A., Courbeyrette, R., Rambourg, A., and Jackson, C.L. (2001). The ARF exchange factors Gea1p and Gea2p regulate Golgi structure and function in yeast. J. Cell Sci. **114:** 2241–2253.

Peyroche, A., Antonny, B., Robineau, S., Acker, J., Cherfils, J., and Jackson, C.L. (1999). Brefeldin A acts to stabilize an abortive ARF-GDP-Sec7 domain protein complex: involvement of specific residues of the Sec7 domain. Mol. Cell **3:** 275–285.

Pimpl, P., Movafeghi, A., Coughlan, S., Denecke, J., Hillmer, S., and Robinson, D.G. (2000). In situ localization and in vitro induction of plant COPI-coated vesicles. Plant Cell **12:** 2219–2236.

Richter, S., Geldner, N., Schrader, J., Wolters, H., Stierhof, Y.D., Rios, G., Koncz, C., Robinson, D.G., and Jürgens, G. (2007). Functional diversification of closely related ARF-GEFs in protein secretion and recycling. Nature **448:** 488–492.

Robinson, D.G., Jiang, L., and Schumacher, K. (2008). The endosomal system of plants: charting new and familiar territories. Plant Physiol. **147:** 1482–1492.

Robinson, D.G., Scheuring, D., Naramoto, S., and Friml, J. (2011). ARF1 localizes to the golgi and the trans-Golgi network. Plant Cell **23:** 846–849, author reply 849–850.

Shevell, D.E., Kunkel, T., and Chua, N.H. (2000). Cell wall alterations in the Arabidopsis emb30 mutant. Plant Cell **12:** 2047–2060.

Shevell, D.E., Leu, W.M., Gillmor, C.S., Xia, G., Feldmann, K.A., and Chua, N.H. (1994). EMB30 is essential for normal cell division, cell expansion, and cell adhesion in Arabidopsis and encodes a protein that has similarity to Sec7. Cell **77:** 1051–1062.

Someya, A., Sata, M., Takeda, K., Pacheco-Rodriguez, G., Ferrans, V.J., Moss, J., and Vaughan, M. (2001). ARF-GEP(100), a guanine nucleotide-exchange protein for ADP-ribosylation factor 6. Proc. Natl. Acad. Sci. USA **98:** 2413–2418.

Spitzer, C., Reyes, F.C., Buono, R., Sliwinski, M.K., Haas, T.J., and Otegui, M.S. (2009). The ESCRT-related CHMP1A and B proteins mediate multivesicular body sorting of auxin carriers in Arabidopsis and are required for plant development. Plant Cell **21:** 749–766.

Staehelin, L.A., and Kang, B.H. (2008). Nanoscale architecture of endoplasmic reticulum export sites and of Golgi membranes as determined by electron tomography. Plant Physiol. **147:** 1454–1468.

Steinmann, T., Geldner, N., Grebe, M., Mangold, S., Jackson, C.L., Paris, S., Gälweiler, L., Palme, K., and Jürgens, G. (1999). Coordinated polar localization of auxin efflux carrier PIN1 by GNOM ARF GEF. Science **286:** 316–318.

Tanaka, H., Kitakura, S., De Rycke, R., De Groodt, R., and Friml, J. (2009). Fluorescence imaging-based screen identifies ARF GEF component of early endosomal trafficking. Curr. Biol. **19:** 391–397.

Tartakoff, A.M. (1983). Perturbation of vesicular traffic with the carboxylic ionophore monensin. Cell **32:** 1026–1028.

Teh, O.K., and Moore, I. (2007). An ARF-GEF acting at the Golgi and in selective endocytosis in polarized plant cells. Nature **448:** 493–496.

Tian, G.W., et al. (2004). High-throughput fluorescent tagging of full-length Arabidopsis gene products in planta. Plant Physiol. **135:** 25–38.

Ueda, T., Uemura, T., Sato, M.H., and Nakano, A. (2004). Functional differentiation of endosomes in Arabidopsis cells. Plant J. **40:** 783–789.

Uemura, T., Suda, Y., Ueda, T., and Nakano, A. (2014). Dynamic behavior of the trans-golgi network in root tissues of Arabidopsis revealed by super-resolution live imaging. Plant Cell Physiol. **55:** 694–703.

Viotti, C., et al. (2010). Endocytic and secretory traffic in Arabidopsis merge in the trans-Golgi network/early endosome, an independent and highly dynamic organelle. Plant Cell **22:** 1344–1357.

Wood, S.A., Park, J.E., and Brown, W.J. (1991). Brefeldin A causes a microtubule-mediated fusion of the trans-Golgi network and early endosomes. Cell **67:** 591–600.

Xu, J., and Scheres, B. (2005). Dissection of Arabidopsis ADP-RIBOSYLATION FACTOR 1 function in epidermal cell polarity. Plant Cell **17:** 525–536.

Zeghouf, M., Guibert, B., Zeeh, J.C., and Cherfils, J. (2005). Arf, Sec7 and Brefeldin A: a model towards the therapeutic inhibition of guanine nucleotide-exchange factors. Biochem. Soc. Trans. **33:** 1265–1268.

Zhang, G.F., Driouich, A., and Staehelin, L.A. (1993). Effect of monensin on plant Golgi: re-examination of the monensin-induced changes in cisternal architecture and functional activities of the Golgi apparatus of sycamore suspension-cultured cells. J. Cell Sci. **104:** 819–831.